

Diffuse reflectance spectra and optical properties of some sulphides and related minerals

B. J. WOOD

Department of Geology, The University, Manchester M13 9PL

R. G. J. STRENS

School of Physics, The University, Newcastle upon Tyne NE1 7RU

SUMMARY. The results of measurements of diffuse reflectance over the wavelength range $200 < \lambda < 2500$ nm are reported for sphalerite, cinnabar, alabandite, chalcocopyrite, bornite, orpiment, stibnite, bismuthinite, enargite, and pyrargyrite, and for eight pyrite-type and four NiAs-type compounds. Some spectral assignments have been made.

Optical properties are related to the absorption spectrum (and through this to composition and structure) in a rational way. Absolute reflectances tend to increase with mean atomic number (z) through the operation of the 'z-sum rule', and at constant z they decrease as the band gap increases. Bireflectance is structurally controlled, being weak in derivatives of the cubic sphalerite and pyrite structures, moderate in derivatives of wurtzite and NiAs, and strong in anisodesmic structures such as that of stibnite. Extreme bireflectance occurs in anisodesmic structures with strong dichroic absorption bands in the visible (molybdenite, covelline).

The dispersion of reflectance ($dR/d\lambda$) depends on the position of the centre of the main absorption envelope ($\bar{\lambda}$) in relation to the visible spectrum. For $\lambda > \bar{\lambda}$, dispersion is normal ($R_{\text{blue}} > R_{\text{red}}$, $dR/d\lambda$ negative), the streak is light or coloured, and polished surfaces tend to be bluish. For $\lambda < \bar{\lambda}$, dispersion is reversed ($R_{\text{red}} > R_{\text{blue}}$), the streak is dark, and polished surfaces are yellowish. Polished surfaces are white or grey if absorption varies little through the visible or strongly coloured if it varies rapidly (covelline, chalcocopyrite).

THE spectra and optical properties of both transparent and opaque minerals are linked by dispersion equations, of which the Helmholtz (Strens and Freer, 1978) and Kramers-Kronig (Harbeke, 1968) are the most useful, so that the two subjects are best considered together. The spectra also provide information about the electronic energy levels of the mineral, and these in turn define its physical properties and chemical reactions.

Diffuse reflectance spectroscopy is a rapid reconnaissance technique that locates the main regions of absorption and provides information on the energy, width, and intensity of absorption

bands. A brief critical review, which includes details of experimental procedures, is given by Strens and Wood (1979). A more detailed discussion is that by Wendlandt and Hecht (1966). Specular reflectance methods have been reviewed by Strens (1979).

The original spectra, in the form of plots of diffuse reflectance (r) against photon energy, are given by Wood (1971). They have been converted to plots of the Kubelka-Munk function $f(r)$ against wavelength (λ in nm) and photon energy ($h\nu$ in eV), $f(r)$ being defined by:

$$f(r) = \frac{(1-r)^2}{2r} \approx \frac{k}{s} \quad (1)$$

where k and s are absorption and scattering coefficients respectively. Because s varies slowly with wavelength, $f(r)$ provides a good representation of the absorption spectrum of the material.

Three problems arise in using these spectra. First, some sulphides are susceptible to surface oxidation, and reflectance methods measure surface rather than bulk properties; secondly, for anisotropic minerals the method preferentially records the spectrum of the least absorbing orientation; and thirdly, the ratio k/s is underestimated at high k , with $f(r)$ values above about 50 being unreliable. This work should thus be regarded as a reconnaissance of the spectra, and not as a definitive survey.

The specular reflectances at normal incidence (R) of minerals in the visible region (400–700 nm) have been taken from the first edition of the Quantitative Data File (QDF) of the IMA-COM, edited by N. F. M. Henry (1977), and reference to these is by card number, e.g. QDF 1.7100. Refractive indices, usually measured by minimum deviation, have been taken from the Landolt-Börnstein (LB) Tables, compiled by S. Koritnig (1962). Magnetic and electrical data are from Vaughan and Craig (1978).

The spectra are considered in three groups. The

first comprises compounds of ions having stable closed-shell electronic configurations, e.g. S^{2-} (Ar), As^{3-} (Kr), Sb^{3-} (Xe), Cu^+ and Zn^{2+} (Ar) $3d^{10}$, Hg^{2+} (Xe) $5d^{10}$. These compounds are diamagnetic semiconductors with band gaps (E_g) of 0.5 to 3.6 eV, having specular reflectances that decrease monotonically with photon energy below E_g . Some are transparent (ZnS), while others are strongly coloured (HgS) or opaque (Sb_2S_3) depending on the magnitude of the band gap. Compounds containing transition metal ions with relatively stable half-filled d -shells, e.g. α -MnS and chalcopyrite, behave similarly.

The second group includes derivatives of the pyrite structure MX_2 , with $M = Fe, Co, Ni$ and $X_2 = S_2, As_2$ or AsS . These range from diamagnetic semiconductors (FeS_2) to semi metals ($FeAs_2$) according to the electronic configuration of the transition metal ion, and all have high specular and low diffuse reflectance throughout the visible region.

The last group includes derivatives of the NiAs structure MX , with $M = Fe, Ni$ and $X = S, As$. Most are metallic, although the properties range from semiconducting antiferromagnetic (troilite) to metallic and Pauli paramagnetic (NiAs). Diffuse reflectances are low. Specular reflectances are high, and they increase from blue to red.

Spectra and optics of closed-shell compounds

The spectra of closed-shell compounds display regions of low and high diffuse reflectance. At low photon energies, the material is transparent with high diffuse and low specular reflectance, while at high photon energies the reverse is true, and the material is opaque. Between these regions at an energy just below that of the band gap (E_g), lies the absorption edge. We define the optical band gap E_g by extrapolating the linear part of the absorption edge to the $f(r)$ value of the first major absorption maximum on the high-energy side of the edge, and determining the resulting E_g .

The origin of the band gap, and its dependence on composition and covalency, are illustrated by applying the Born-Haber cycle to the combination of sodium and iodine to form the strongly ionic compound sodium iodide. Sodium and iodine have the electronic configurations (Ne) $3s^1$ and (Kr) $4d^{10}5s^25p^5$ respectively. Sodium easily loses its $3s$ electron (ionization potential 5.14 eV) and iodine accepts it (electron affinity 3.45 eV) to give the stable closed-shell configurations of the ions Na^+ (Ar) and I^- (Xe). Combination of these ions to give NaI releases 7.2 eV, so that the energy of formation of the compound from its elements is (5.14 - 3.45) - 7.2 = -5.5 eV. The photon energy required to

transfer the sixth p -electron of I^- to the sodium, i.e. the energy difference between the filled valence orbital of the anion and the empty valence orbital of the cation is equal to the energy released on combination (5.5 eV). This defines the band gap, which is observed experimentally at $E_g = 5.7$ eV. In covalent materials, the effective charges on the cationic and anionic species are lower, thus reducing the energy needed to transfer an electron between them. In TII, the band gap is calculated at 4.24 eV and observed at 3.1 eV. In AgI, the corresponding figures are 4.6 and 3.1 eV, clearly displaying the effect of increasing covalency in the sequence NaI-TII-AgI.

Batsonov (1964) has derived the following equation relating E_g of a semiconductor to the electronegativity and position in the periodic table of its constituents:

$$E_g = \bar{E}_a + \bar{E}_c + A(\bar{X}_a - \bar{X}_c) - B(\bar{N}_a - N_c) \quad (2)$$

where \bar{E}_a and \bar{E}_c are the mean band gaps of the anionic and cationic elements, \bar{X}_a and \bar{X}_c are their mean electronegativities, and \bar{N}_a , N_c their mean periods, all weighted according to the composition. For sulphides, the constants $A = 5.3$, $B = 1.3$ give generally satisfactory agreement with observed values, except for HgS, which is unusual in having a linearly coordinated cation. These results, and consideration of the spectra and electrical properties suggest that the valence electrons of the anions are delocalized over the cation sublattices in most of the closed-shell sulphides, but that electrons associated with the cations are often localized, at least on the time scale of the optical transitions.

Cinnabar, chalcopyrite, bornite, orpiment, stibnite, enargite, and pyrargyrite were obtained from the collections of the Department of Geology, University of Newcastle upon Tyne. The remaining phases were prepared by direct combination of the elements at 450 °C, followed by grinding, and further reaction of pressed pellets of the partially reacted material for a week at 450 °C. The phase purity of both natural and synthetic samples was confirmed by X-ray diffraction.

Binary compounds

Sphalerite (ZnS: $F\bar{4}3m$). Sphalerite is the parent of a large family of polymeric isomorphs derived by coupled substitutions of other elements for zinc ($CuFeS_2$), by omission of cations or anions ($\square Al_2ZnS_4$; $Ag_3SbS_3\square$), or by entry of excess cations into interstitial positions (Cu_3FeS_4). Like sphalerite, these derivative phases are semiconductors, many belonging to enantiomorphous or acentric point groups capable of displaying optical activity, non-linear behaviour or both.

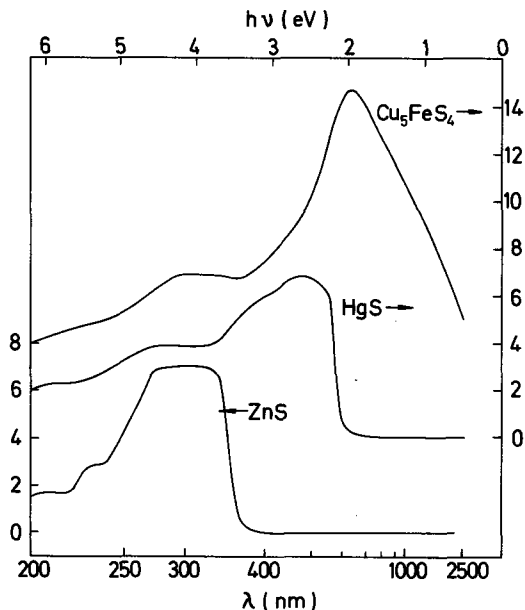


FIG. 1. Diffuse reflectance spectra of natural sphalerite, cinnabar, and bornite showing the variation of $f(r) \approx k/s$ as defined in equation (1) with photon energy and wavelength. The arrows indicate the $f(r)$ scale to be used. The well-defined absorption edges of ZnS and HgS separate regions of high (> 1) and low (≤ 1) absorption. The band gap of bornite apparently lies below 0.5 eV (2500 nm).

The spectrum of sphalerite (fig. 1) has a well-defined absorption edge, with $E_g = 3.6$ eV (346 nm), so that the pure synthetic material is colourless. Natural material is often coloured by impurities, of which Fe^{2+} is the most important, $d-d$ transitions of this ion being responsible for absorption near 0.425 eV.

Accurate index dispersion data (LB 212) fit a Sellmeier dispersion equation with $\lambda_0 = 201.2$ nm, which compares with $\bar{\lambda} = 290$ nm. We expect $\bar{\lambda} > \lambda_0$ because of the effect on the index of absorption bands below 200 nm. The specular reflectances (QDF I.8100) agree with those calculated from the observed indices and they follow a dispersion equation obtained by substituting the Sellmeier expression for n (Strens and Freer, 1978) into the Fresnel relation for reflectance at normal incidence:

$$(3) \quad R(\%) = 100 \frac{((1 + IL/\pi^2)^{\frac{1}{2}} - 1)^2}{((1 + IL/\pi^2)^{\frac{1}{2}} + 1)^2}$$

where I and λ_0 are the integrated absorbance and mean wavelength of the bands contributing to the dispersion, and $L = \lambda^2/(\lambda^2 - \lambda_0^2)^2$. Absolute reflectance is low (16.4% at 589 nm) because of the large band gap and low mean atomic number. Sphalerite, being cubic, is isotropic.

Cinnabar (HgS: P3121). Cinnabar has a unique structure built of helical S-Hg-S chains cross-linked by weak Hg-S bonds to neighbouring chains, so that Hg^{2+} has 2+4 coordination, and may be regarded to a first approximation as linearly sp -hybridized. The helical chains give rise to the optical rotation for which cinnabar is noted, and which has caused its properties to be studied with unusual thoroughness.

The spectrum (fig. 1) qualitatively resembles that of sphalerite, but the band gap is smaller (2.2 eV), so that diffuse reflectance is high in the red, and low below about 565 nm. This, and the high refractive index, accounts for the brilliant red colour of the powder.

The indices have been determined to five decimal places from 589 to 762 nm (LB 218), and they fit a Sellmeier dispersion equation with $\lambda_0 = 299$ nm (ω) and 312 nm (ϵ), compared with $\bar{\lambda} = 420$ nm for the centre of the major absorption band in the blue. Dispersion of R_e follows equation (3) to an energy well above the band gap (fig. 2), the agreement for R_o being poorer. Reflectances calculated from the indices are higher than observed reflectances (QDF I.1620), possibly due to the formation of an oxide layer on polished surfaces.

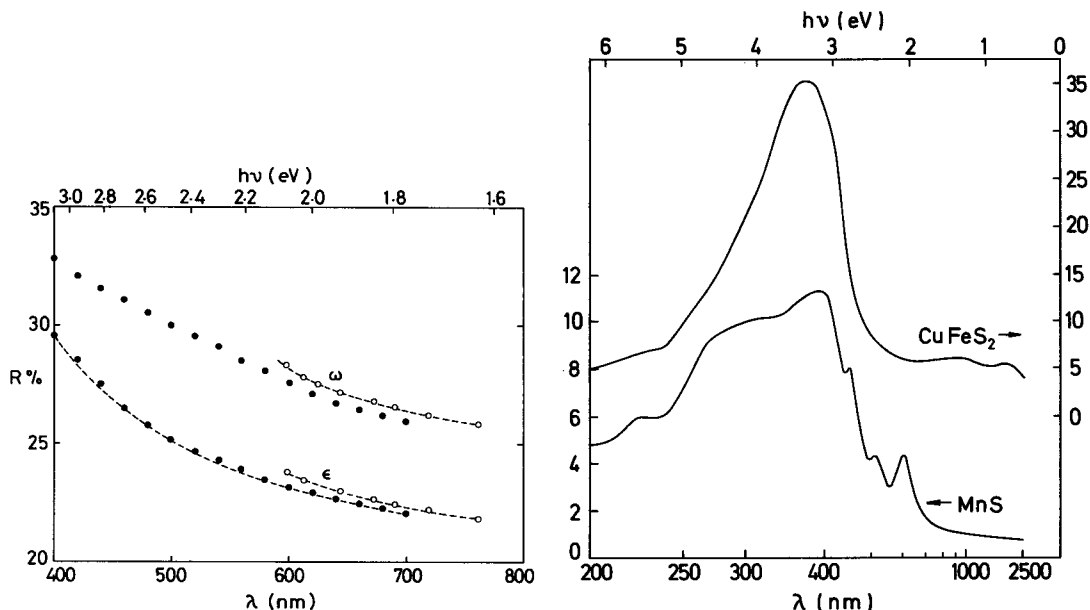
Absolute reflectance at 589 nm ($R_o = 27.8\%$) is higher than that of sphalerite because of the smaller band gap and larger mean atomic number. Relative bireflectance $(R_o - R_e)/R_o = 16\%$ at 589 nm. The very large optical rotation ($325^\circ/\text{mm}$ at 671 nm) is attributed to the proximity of the absorption edge, rotation increasing exponentially as $h\nu \rightarrow E_g$ (Newnham, 1975, fig. 54).

Alabandite ($\alpha\text{-MnS}$: $Fm\bar{3}m$). Alabandite is an antiferromagnetic semiconductor with the sodium chloride structure, Mn^{2+} being octahedrally coordinated by sulphur. The spectrum (fig. 3) of synthetic alabandite shows a well-defined band gap of 3.1 eV (400 nm), with three spin-forbidden transitions of Mn^{2+} superimposed on the absorption edge. These were assigned by Wood (1971) as follows:

$${}^6A_1 - {}^4T_1 \quad 2.01; \quad {}^6A_1 - {}^4T_2 \quad 2.43; \quad {}^6A_1 - {}^4A_1 \quad 2.70 \text{ eV.}$$

Using the approximation $C = 4B$ for the configuration interaction term B^2/Δ , he found for the Racah parameters $B = 0.0645$, $C = 0.403$, $\Delta = 0.905$ eV. The green colour of the powder is caused by the presence of a diffuse reflectance peak (absorption minimum) in the green between the absorption edge and the ${}^6A_1 - {}^4T_1$ transition.

There appear to be no index dispersion data, but the reflectances (QDF I.0120) decrease monotonically from blue to red, as expected for a material with $\bar{\lambda} \approx 320$ nm.



FIGS. 2 and 3. FIG. 2 (left). Dispersion of specular reflectance (R) for the ω and ϵ vibrations in cinnabar (HgS). Solid symbols (\bullet) represent specular reflectances measured at normal incidence, open symbols (\circ) those calculated from measured refractive indices using the Fresnel relation, and dashed lines the dispersion curves calculated using equation (3). FIG. 3 (right). Diffuse reflectance spectra of synthetic alabandite (α - MnS) and natural chalcopyrite. Arrows indicate the $f(r)$ scale to be used. Sharp $d-d$ bands of Mn^{2+} are superimposed on the absorption edge of alabandite and an absorption minimum (transmission window) occurs in the green at about 540 nm. The absorption edge of chalcopyrite lies below 0.5 eV.

Chalcopyrite (CuFeS_2 ; $I\bar{4}2d$) and *bornite* (Cu_5FeS_4 ; $Pbca$). The structure of chalcopyrite is derived from that of sphalerite by replacing alternate zinc atoms by copper and iron. That of bornite is the result of both coupled replacement of zinc by Cu^+ and Fe^{3+} , and the substitution of Cu^+ into tetrahedral sites not occupied in sphalerite. Both minerals are semiconducting, chalcopyrite being antiferromagnetic, while bornite, which has a lower density of magnetic (Fe^{3+}) ions, is paramagnetic.

Both minerals tarnish readily, and we think it unwise to attempt a detailed interpretation of their spectra (figs. 1, 3). Strong absorption is present from 200 to 2500 nm, so that the optically defined band gaps are less than about 0.5 eV, and the powder (streak) is dark. Specular reflectances (QDF 1.1500, 1.1020) increase sharply from blue to red, the rapid change in reflectance of chalcopyrite at about 470 nm (Araya *et al.*, 1977) possibly being connected with the increase in $f(r)$ in this region (fig. 3). The reverse dispersion gives polished surfaces a yellow tint, particularly noticeable in chalcopyrite. Bireflectance is small, with R_e 47.6, R_o 46.6% at 580 nm in chalcopyrite.

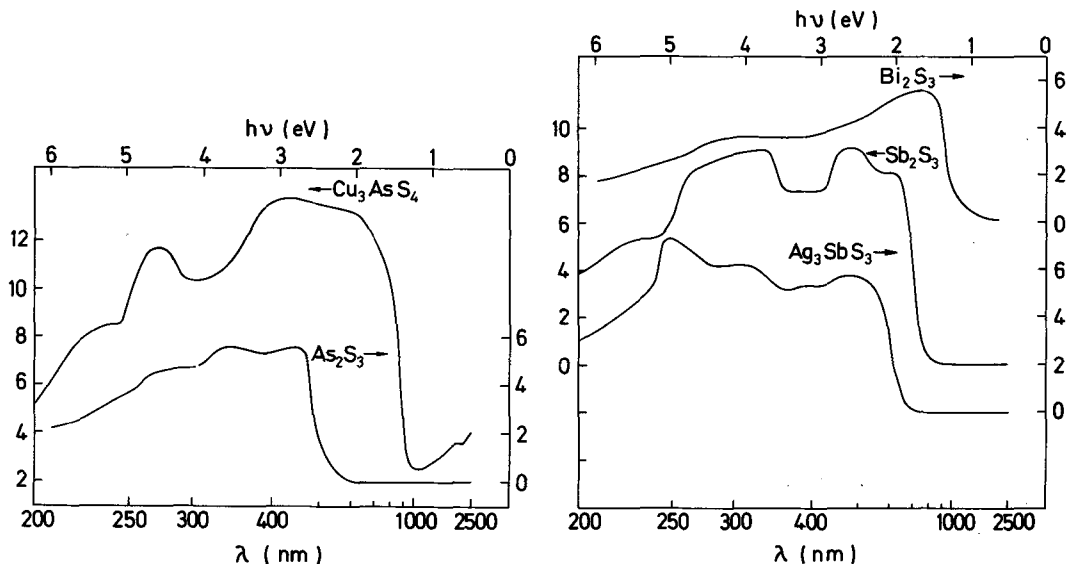
Orpiment (As_2S_3 ; $P2_1/m$). Orpiment has a structure in which $[\text{AsS}_3]$ groups share sulphurs to form corrugated sheets normal to the unique axis (b). The spectrum (fig. 4) shows a well-defined absorption edge with $E_g = 2.57$ eV.

The brilliant yellow colour of the powder (streak) has a complex origin. The brilliance is attributable to the high scattering resulting from the high refractive index ($n \approx 3$). The colour results from a combination of the low diffuse reflectance in the blue, the high diffuse reflectance in the yellow and red, and the greater sensitivity of the eye to yellow than to blue or red light.

Specular reflectances (QDF 1.6300) decrease monotonically from blue to red, and they are well approximated by equation (3) with $\lambda_0 = 302$ nm. Bireflectance is strong (18% at 580 nm).

Stibnite (Sb_2S_3 ; $Pbnm$) and *bismuthinite* (Bi_2S_3 ; $Pbnm$). Stibnite and bismuthinite share a complex structure based on double chains of composition $[\text{Sb}_4\text{S}_6]_n$ parallel to the short b axis. Their spectra (fig. 5) show well-defined absorption edges with $E_g = 1.66$ (stibnite) and 1.43 eV (bismuthinite).

Specular reflectance data for stibnite (QDF 1.8420) show $R_c = 45.8$, $R_a = 40.7$, $R_b = 30.3\%$ at



FIGS. 4 and 5. FIG. 4 (left). Diffuse reflectance spectra of natural orpiment and enargite. Arrows indicate the $f(r)$ scale to be used. Both minerals have well-defined absorption edges, that of enargite being modified by $d-d$ absorption of tetrahedral Fe^{2+} impurities just below 0.5 eV. FIG. 5 (right). Diffuse reflectance spectra of natural stibnite and pyrrargyrite, and of synthetic bismuthinite. The arrows indicate the $f(r)$ scale to be used.

580 nm, so that the lowest reflectance is that for \mathbf{E}/b , the chain axis. Absolute reflectance is high, and relative bireflectance very strong, $(R_c - R_b)/R_c = 34\%$. The dispersion equation (3) fits R_c to energies well above the band gap, and there is very good agreement between observed reflectances and those calculated from the refractive indices (LB 236). The lowest reflectances (R_a , R_b) do not obey equation (3), and the spectra suggest absorption at 510 and 670 nm.

Reflectance data for bismuthinite are sparse (QDF 1.0920), but it is clear that the bireflectances are much lower than those of stibnite, although absolute reflectances are comparable. Dispersion of reflectance is small, and equation (3) probably does not apply in the visible region.

Ternary compounds

Enargite (Cu_3AsS_4 : $Pnm2$). The structure of enargite is derived from that of wurtzite (ZnS) by the ordered replacement of 4Zn by Cu_3As , and the ordered omission of one-quarter of the sulphur atoms: it is unusual in having arsenic tetrahedrally coordinated by sulphur. The spectrum of the natural mineral (fig. 4) shows a well defined absorption edge ($E_g = 1.46$ eV), and the onset of absorption by tetrahedral Fe^{2+} near 0.5 eV. Specular reflectance data (QDF 1.2500) display only slight irregular dispersion of reflectance, and moderate relative bireflectance.

Proustite (Ag_3AsS_3 : $R3c$) and **pyrrargyrite** (Ag_3SbS_3 : $R3c$). These structures are derived from that of sphalerite by replacement of 4Zn by Ag_3As or Ag_3Sb , and by omission of one-quarter of the sulphur atoms. The spectrum of pyrrargyrite (fig. 5) shows a well defined absorption edge, with a band gap in the visible ($E_g = 2.05$ eV, $\lambda_g = 606$ nm), so that some red light is transmitted by thin sections, and the powder is red. The diffuse reflectance spectrum of proustite was not recorded, but it is clear from both index (LB 210) and specular reflectance (QDF 1.7100, 1.7040) data that their properties are very similar, the optics of both being quite well represented by equation (3) with $\lambda_0 \approx 320$ nm. Bireflectance is weak.

Pyrite-type compounds

There are many compounds of formula MX_2 , MXY , and MY_2 (where M is a transition metal, and X , Y are elements of groups V(b) and VI(b) respectively) crystallizing with the pyrite or marcasite, arsenopyrite, and löllingite structures. In all these compounds, the transition metal ions are octahedrally coordinated by six X_2 , XY or Y_2 dianions. In pyrite, neighbouring octahedra share corners, while in marcasite and arsenopyrite each octahedron shares two edges. In marcasite (FeS_2) the Fe-Fe distances are equal at 3.38 Å. In arsenopyrite (FeAsS), short (2.89 Å) and long (3.53 Å) distances alternate, while in the distorted marcasite structure

of löllingite (FeAs_2) the Fe-Fe distances are short (2.85 Å).

The X and Y atoms are coordinated by $3M+X$ or $3M+Y$, and may be regarded as sp^3 hybridized to form filled bonding orbitals with closed-shell configurations $(\text{S}_2)^{2-}$, $(\text{AsS})^{3-}$ and $(\text{As}_2)^{4-}$. These filled orbitals overlap with the metal e_g orbitals, destabilizing the latter, and causing spin-pairing in cations with 4–7 d -electrons, and the formation of an e_g conduction band which is responsible for metallic conduction in compounds of d^7 and d^9 ions with a single electron or hole in the e_g band.

The formal negative charges of 2, 3, and 4 on S_2 , AsS , and As_2 dianions require formal positive charges of 2, 3, and 4 on the Fe ions in pyrite, arsenopyrite, and löllingite respectively. These charges are in agreement with the results of measurements of magnetic susceptibility.

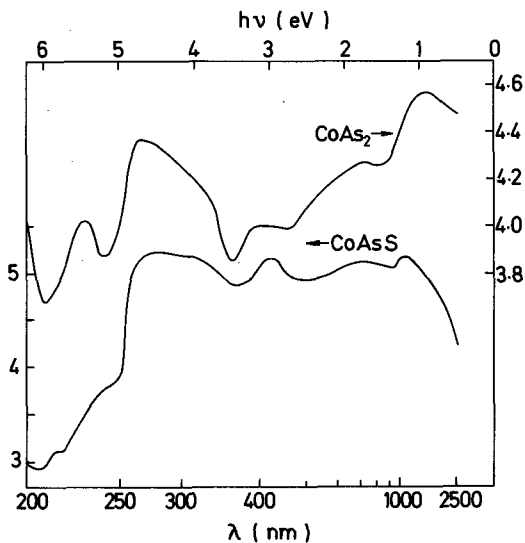
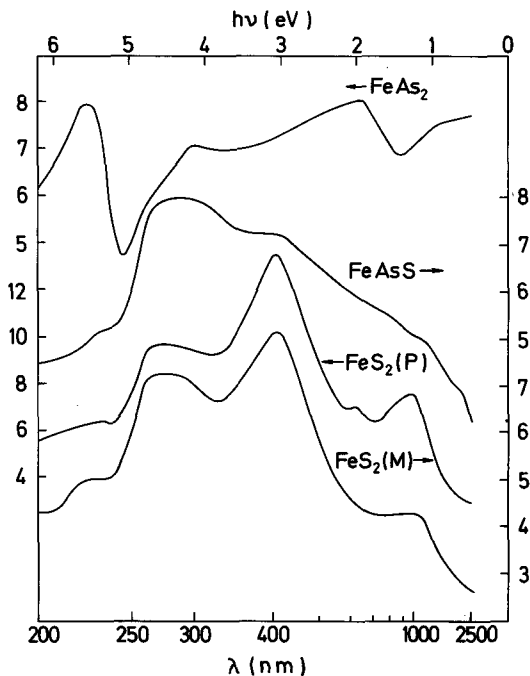
It follows from the structures and electronic configurations that the spectra will be very difficult to interpret, with contributions from $d-d$ transitions of the metal ions, internal transitions of the dianions, and metal-ligand charge transfer. There will also be absorption by free electrons in the metallic compounds. Because of this complexity, we have not attempted detailed assignments of the

spectra, merely noting some possible assignments of important spectral features with emphasis on $d-d$ transitions (Wood, 1971) and internal transitions of the dianions.

Previous work by Bither *et al.* (1968), Goodenough (1972), Wilson and Yoffe (1969), and others has been reviewed by Vaughan and Craig (1978). Molecular orbital calculations are available for pyrite (Tossell, 1977) and for the dianions S_2 , AsS and As_2 (Dempsey, pers. comm. 1978).

Natural pyrite, marcasite, and arsenopyrite were obtained from the collections of the Geology Department, University of Newcastle upon Tyne. The remaining phases were synthesized by direct combination of the elements near the boiling point of sulphur, followed by grinding and further reaction. The purity of the samples was checked by X-ray diffraction.

Pyrite (FeS_2 : Pa_3) and marcasite (FeS_2 : $Pnmm$). Both pyrite and marcasite are diamagnetic semiconductors with electrical band gaps of about 0.9 eV, implying that Fe^{2+} (d^6) is spin-paired with $^1A_{1g}$ ground state. The spectra are very similar (fig. 6), and the first four bands (only three of which are visible on the $f(r)$ plot) were assigned by Wood (1971) to the $d-d$ transitions $^1A_1-^3T_1$ (0.81), $^1A_1-^1T_1$ (1.30), $^1A_1-^1T_2$ (1.96) and $^1A_1-^1E$ (3.0 eV) using



FIGS. 6 and 7. FIG. 6 (left). Diffuse reflectance spectra of natural pyrite (P), marcasite (M), and arsenopyrite and of synthetic löllingite. Arrows indicate the $f(r)$ scale to be used. FIG. 7 (right). Diffuse reflectance spectra of synthetic cobaltite (CoAsS) and safflorite (CoAs_2). Arrows indicate the $f(r)$ scale to be used.

a Tanabe-Sugano diagram with $B \approx 0.053$ and $\Delta \approx 1.43$ eV. On this view, the activation energy for semiconduction corresponds to the lowest energy transition to the e_g conduction band.

Tossell (1977) used molecular orbital calculations to assign bands in the specular reflectance spectra of pyrite to $M-S_2$ charge-transfer (0.5 eV), a $d-d$ transition (1.9 eV), and internal transitions of the S_2 dianion (4–6 eV). Dempsey's calculations for S_2^{2-} suggest that strong absorption by isolated S_2^{2-} dianions would occur near 3.5 ($\pi_g-\sigma_u$) and 5.8 eV ($\pi_u-\sigma_g$). It must be remembered that reflectance peaks do not in general coincide with the centres of absorption bands, and that Dempsey's figures will be increased by up to 1 eV when transition-state calculations are completed.

Both pyrite and marcasite display moderate to strong reverse dispersion of the specular reflectances (QDF 1.7120, 1.5400). Pyrite is isotropic, but marcasite has moderate relative bireflectance.

Arsenopyrite ($FeAsS$: $P2_1/c$). Arsenopyrite is a semiconductor with a very low magnetic moment, implying that adjacent pairs of Fe^{3+} ions are bonded, consistent with the alternating short and long Fe-Fe distances. The featureless spectrum (fig. 6) may reflect band broadening by this interaction, and suggests $E_g < 0.5$ eV, compared with an electrically determined value of 0.4 eV. Specular reflectance data (QDF 1.0520) show slight reverse dispersion, and weak bireflectance.

Löllingite ($FeAs_2$: $Pnmm$). Löllingite is a diamagnetic semiconductor in which structural distortions destabilize the d_{xy} orbital of the cation, reducing the Fe-Fe separation, and causing complete spin pairing in the d_{xz} , d_{yz} (1E) ground state. The extreme distortion forbids use of the Tanabe-Sugano diagram to assign such bands as are visible in the spectrum (fig. 6), but $d-d$ transitions may be responsible for features near 0.5 and 4 eV. The least energetic transition would presumably be from 1E to a delocalized d_{xy} or d_{z^2} orbital, accounting for the electrically determined band gap of 0.2 eV.

Dempsey's calculations suggest absorption by the As_2^{2-} dianion at energies somewhat above 2.4 ($\pi_g-\sigma_u$), 3.3 ($\pi_u-\sigma_g$) and 4.8 eV ($\pi_u-\Delta_g$). It is tempting to assign the band at 5.5 eV in the spectra of the two diarsenides studied (löllingite, fig. 6, safflorite, fig. 7) to the $\pi_u-\Delta_g$ transition, as it is absent from the spectra of the disulphides and sulpharsenides.

The specular reflectances of löllingite (QDF 1.4980) show slight normal dispersion and weak bireflectance, the latter supporting the view that the short Fe-Fe distances along c are caused not by Fe-Fe bonding but by a reduction in repulsion between d_{xy} electrons when these orbitals are emptied by spin-pairing (Pearson, 1965). Inter-

metallic bonding should cause metallic conduction in this direction, increasing R_c considerably.

Cobaltite ($CoAsS$: $Pa3$). Cobaltite is isoelectronic with pyrite and marcasite, and bands at 0.74, 1.21, 1.61, and 3.0 eV (fig. 7) were assigned by Wood (1971) to the $^1A_1-^3T_1$, $^1A_1-^1T_1$, $^1A_1-^1T_2$ and $^1A_1-^1E$ transitions of Co^{3+} (d^6), using a Tanabe-Sugano diagram with $B = 0.048$, $\Delta = 1.3$ eV. The band gap should be defined by the spin-forbidden $^1A_1-^3T_1$ transition at 0.75 eV. As in the isoelectronic phases pyrite and marcasite, cobaltite has reverse dispersion of specular reflectance (QDF 1.1660) and weak bireflectance.

Safflorite ($CoAs_2$: $Pnmm$). Safflorite is isoelectronic with arsenopyrite, which it resembles in structure and in electrical and magnetic properties. Bands at about 1.2 and 3 eV (fig. 7) may be of $d-d$ origin and that at about 5.5 eV may represent the $\pi_u-\Delta_g$ transition of the As_2 dianion. No QDF data are available.

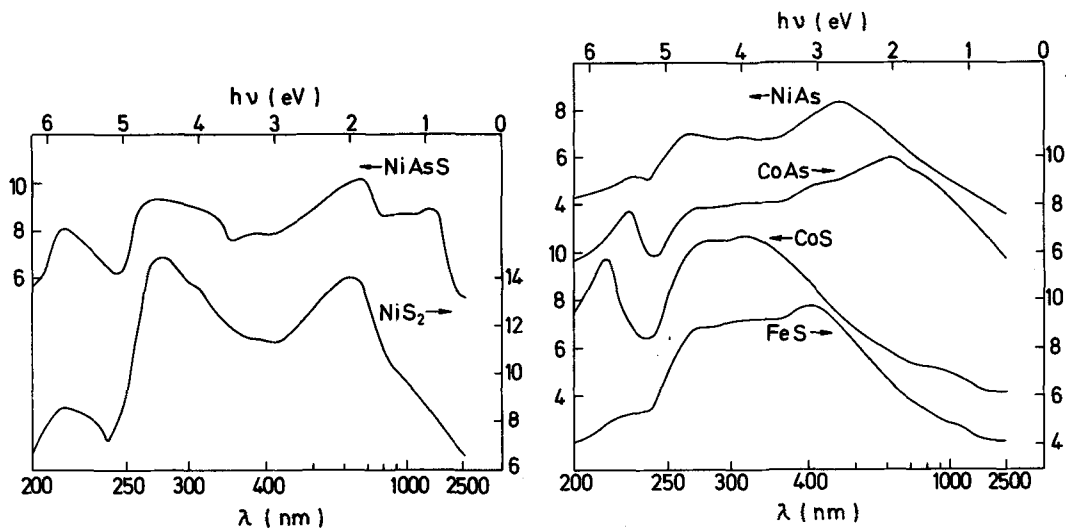
Vaesite (NiS_2 : $Pa3$). Vaesite is an antiferromagnetic semiconductor with a d^8 (3A_2) ground state. The contrast with the semimetallic properties of the d^7 and d^9 pyrites is attributable to spin-splitting of the e_g conduction band in the latter, which restricts metallic conduction to materials with a single hole in either spin-up or spin-down bands (VC 169).

Wood (1971) assigned the bands at about 1.25 and 2.0 eV (fig. 7) to the $^3A_2-^3T_2$ and $^3A_2-^3T_1$ transitions, finding $B = 0.077$, $\Delta = 1.26$ eV. No QDF data are available.

Gersdorffite ($NiAsS$: $Pa3$ or $P2_13$). Gersdorffite is a d^7 pyrite with a 2E ground state, isoelectronic with CoS_2 , six electrons being localized in the t_{2g} levels, with the seventh half-filling one of the spin-split e_g conduction bands, and conferring semimetallic properties. Wood (1971) tentatively assigned bands near 0.9, 1.9, 3.4, 4 eV (fig. 8) to the $^2E-^4T_1$, $^2E-^2T_1$, 2T_2 $^2E-^4T_1$ (P) and $^2E-^2A_1$ transitions of low-spin Ni^{3+} , finding $B = 0.060$, $\Delta = 2.13$ eV. There is slight reverse dispersion of the reflectance (QDF 1.3080).

NiAs-type compounds

Each arsenic atom in nickeline ($NiAs$) is bonded to six nickel atoms at the apices of a trigonal prism with its triad axis parallel to c . Each nickel atom is octahedrally coordinated by arsenic, the $[NiAs_6]$ octahedra sharing faces along the c -axis, resulting in a Ni-Ni separation of only 2.52 Å in this direction. As the Ni-Ni distance in metallic nickel is 2.49 Å, this close approach probably implies intermetallic bonding (Wuensch, 1974). The high-temperature phases of FeS, CoS, CoAs, and NiS also adopt the NiAs structure, of which their low-



FIGS. 8 and 9. FIG. 8 (left). Diffuse reflectance spectra of synthetic gersdorffite (NiAsS) and vaesite (NiS₂). Arrows indicate the $f(r)$ scale to be used. FIG. 9 (right). Diffuse reflectance spectra of synthetic NiAs, CoAs, CoS, and FeS. Arrows indicate the $f(r)$ scale to be used.

temperature forms are distorted or non-stoichiometric derivatives.

The spectra of synthetic FeS, CoS, CoAs, and NiAs are shown in fig. 9. Apart from the bands near 5.5 eV in the spectra of CoS and CoAs, the spectra are featureless. Absorption is high, with $f(r) > 4$ to energies below 0.5 eV. The main absorption envelope in the arsenide spectra is wider and extends to lower energies than that in the sulphides.

Intermetallic bonding should increase R_e at low energies, causing reverse dispersion and a decrease in birefractance with increasing wavelength, both of which are present in nickeline ($R_o 44.2$, $R_e 38.4$ at 440 nm, 61.0, 59.9% at 660 nm). The other main source of anisotropy should be the [NiAs₆] prisms, the transitions of which may be either e or o polarized. The balance between these factors will determine the sign of the birefractance, which may be either positive or negative in NiAs derivatives. In nickeline, $R_o > R_e$, but in pyrrhotite $R_e > R_o$ (QDF 1.6061, 1.7240).

Discussion and conclusions

The spectra of the closed-shell sulphides are consistent with the view that the valence electrons of the anions are delocalized over the cation sublattices, so that the electron energies depend on average cation electro-negativities, and the spectrum of a ternary compound is not simply a superposition of the spectra of its binary components.

The presence of narrow and well-defined $d-d$

bands in the spectra of alabandite (α -MnS) and of sphalerite containing Fe²⁺, Co²⁺, Ni²⁺, and Cu²⁺ as impurities (VC 109) is evidence that the d -electrons of these ions are localized on the time scale of the optical transitions. By contrast, only broad $d-d$ bands are seen in the spectra of derivatives of the pyrite structure, in which the t_{2g} electrons appear to be localized, and the e_g electrons are delocalized. In derivatives of the NiAs structure, any $d-d$ bands present have been broadened beyond recognition, reflecting the delocalization of both t_{2g} and e_g electrons, and the magnetic and bonding interactions between metal atoms in these compounds.

The optical properties of opaque minerals are determined by their absorption spectra, and these in turn depend on composition and crystal structure, so that the optical properties are linked with composition and structure in a rational way. Absolute reflectances depend on the dispersive (n) and absorptive (k) constants according to:

$$R(\%) = 100 \frac{(n - \mu)^2 + k^2}{(n + \mu)^2 + k^2} \quad (4)$$

where μ is the refractive index of the transparent immersion medium, and both n and k depend on the numbers and energies of electrons in the system, and thus on spectra, composition and structure. Optical anisotropy is related to the dichroism or pleochroism of the spectra, which is determined by the crystal structure. The colours of polished surfaces and powders (the streak) depend on the

dispersion of specular and diffuse reflectances respectively, and these are determined by the absorption spectrum, and thus by composition and structure.

Absolute reflectances (R) are related by way of the constants n and k to the wavelengths and areas of absorption bands in the spectra by dispersion equations, of which the Helmholtz (Strens and Freer, 1978) and Kramers-Kronig (Harbeke, 1968) relations are the most useful. Thus, equations 5(a) and 5(b) of Strens and Freer relate ε_1 and ε_2 (the real and imaginary parts of the complex dielectric function) to the band areas ($a_i w_i$, where a is the absorption coefficient at band maximum, and w the width at half height) and wavelengths (λ_i):

$$5(a) \quad \varepsilon_1 = n^2 - k^2 = 1 + \frac{1}{2\pi} \sum \frac{a_i w_i \lambda^2}{(\lambda^2 - \lambda_i^2) + w_i^2 \lambda^2 / (\lambda^2 - \lambda_i^2)}$$

$$5(b) \quad \varepsilon_2 = 2nk = \frac{1}{2\pi} \sum \frac{a_i w_i^2 \lambda^3}{(\lambda^2 - \lambda_i^2)^2 + w_i^2 \lambda^2}$$

The sum of all band areas is proportional to the number (z) of electrons in the system (the 'z-sum rule'), so that there is a tendency for the optical constants and reflectances to increase with z , and hence with atomic number. Thus, specular reflectances at 589 nm increase steadily in the series ZnS (16.4), CdS (~19), HgS (~25), HgSe (~30), HgTe (~34), and PbS (43.0), PbSe (49.1), PbTe (67.3). However, much of this change is attributable to the simultaneous reduction in band gap, from 3.6 eV in ZnS and 2.45 eV in CdS to 2.2 eV in HgS, and only detailed study of the spectra can separate the effects of changes in band gap (or λ_i) and z (or $a_i w_i$).

Reflectances thus depend on two quantities, one (z or $a_i w_i$) proportional to the number of electrons involved, and the other (E_g or λ_i) depending on their energies. Neglect of either results in misleading conclusions. For example, Burns and Vaughan (1970) and Vaughan and Craig (1978, fig. 6.1) illustrate what appears to be a good correlation between reflectance at 496 nm in the series FeS₂-CoS₂-NiS₂-CuS₂ and an effective number of electrons (n_{eff}) calculated from the absorption coefficient (k_{496}) at 496 nm. The spectra (fig. 4.5 of Vaughan and Craig, 1978) show that the first major absorption band (E_2) shifts to lower energies with increasing atomic number, from about 1.7 eV (FeS₂) to 1.1, 0.9, and 0.5 eV in CoS, NiS₂, and CuS₂ respectively. This change alone will cause R_{496} to decrease from FeS₂ to CuS₂ as $(\lambda_2 - 496)$ increases. In addition, the contributions of the ($z - n_{\text{eff}}$) other electrons in the system were neglected (which is important when $z = 58$, $n_{\text{eff}} \approx 1.2$ in FeS₂), and

n_{eff} is wrongly calculated from k_{496} rather than the area of the E_2 peak. The apparent correlation between n_{eff} and R is illusory.

Bireflectance is weak to moderate in the non-cubic derivatives of the sphalerite and pyrite structures, the relative bireflectance $(R_{\text{max}} - R_{\text{min}})/R_{\text{max}}$ seldom exceeding 10%. Moderate to strong bireflectance occurs in derivatives of the nickeline and wurtzite structures, particularly those in which magnetic or bonding interactions occur between the metal atoms. Examples are nickeline, cubanite and argentopyrite, in which relative bireflectance approaches 20%.

Strong or very strong bireflectance is typical of anisodesmic structures such as those of orpiment, stibnite, and bismuthinite, in which relative bireflectance reaches 40%. Extreme bireflectance, which is most marked at wavelengths near those of strong dichroic or pleochroic absorption bands, is confined to anisodesmic phases such as graphite, molybdenite (MoS₂), and covellite (Cu₂S.CuS₂). In the layer structure of molybdenite the reflectances at 440 nm are $R_o = 45.8$, $R_e = 20.8\%$ (QDF 1.5820), these extreme values being attributable to a strong ω -polarized doublet centred near 420 nm (Wilson and Yoffe, 1969). Even this extreme bireflectance is exceeded in parts of the covellite spectrum, in which $R_o \approx R_e$ at 700 nm, yet at 620 nm $R_o = 3.55$, $R_e = 21.4\%$ (QDF 1.1920). Strong absorption bands are present at 620 nm (ε) and 710 nm (ω). The assignment of these bands is uncertain, but they presumably arise from transitions of the planar [CuS₃] groups, the triad axes of which are parallel to c (compare the extreme birefringence of calcite, in which CO₃ groups are similarly arranged) or of the S₂²⁻ dianions, with their S-S vectors parallel to c . Contributions from the [CuS₄] tetrahedra should be nearly isotropic.

Dispersion of reflectance in the visible is of three main types. Normally dispersed reflectances ($R_{\text{blue}} > R_{\text{red}}$, $dR/d\lambda$ negative) characterize materials with strong absorption bands centred on the short wavelength side of the visible spectrum, i.e. $\lambda > \bar{\lambda}$ (sphalerite, cinnabar, proustite). Reverse dispersion ($R_{\text{red}} > R_{\text{blue}}$) occurs when the strong absorption lies on the long wavelength side of the visible, i.e. $\lambda < \bar{\lambda}$ (pyrite, nickeline). Irregular dispersion occurs when the visible is a region of strong absorption, i.e. $\lambda \approx \bar{\lambda}$. The reflectance spectrum may be flat and featureless if the absorption remains approximately constant (ilmenite, magnetite), or show distinct structure if it varies rapidly in and near the visible region (chalcopyrite, covellite).

The perceived colour of reflected light depends on the emission spectrum of the source and the sensitivity of the eye as well as the reflectance spectrum of the material, but discounting these

external factors strong normal dispersion gives polished surfaces a bluish tint, examples being digenite ($R = 29.8$ at 400 nm, 16.2% at 700 nm, QDF 1.2260) and proustite ($R_o = 38.5$ at 400 nm, 24.1% at 700 nm, QDF 1.2260). Strong reverse dispersion causes yellow colours, examples being pyrite ($R = 39.3$ at 400 nm, 55.7% at 700 nm, QDF 1.7040) and nickeline ($R_o = 44.2$ at 440 nm, 61.0 at 660 nm, QDF 1.6061). Flat dispersion curves result in white or grey colours (ilmenite, magnetite), while irregular dispersion may cause strong colours (chalcopyrite, covelline).

The streak, that is the colour of a fine powder of the material, depends on the position of the absorption edge in relation to the visible region. This behaviour is caused by the change from low to high diffuse reflectance at the absorption edge (see fig. 1 of Strens and Wood, 1979). If the absorption edge is above 700 nm, the streak is dark (stibnite, enargite, chalcopyrite, pyrite, nickeline); if it is below 400 nm, the streak is light (sphalerite), while minerals with absorption edges in the visible are strongly coloured (cinnabar, orpiment, alabandite, hematite).

The optical properties of opaque minerals are seen to have rational explanations, being determined by the absorption spectra, which in turn depend on the structure and composition of the mineral. The quantitative link between optics and spectra is provided by the dispersion equations, which contain terms describing the volume, composition and orientation dependence (a_i) and wavelength dependence (λ_i, w_i) of the optical constants. Optics and spectra are inseparable, and their understanding should be sought, and taught, together.

Acknowledgements. We thank Dr H. Piller (Carl Zeiss, Oberkochen) and Dr M. J. Dempsey (University of Manchester) for access to their unpublished results.

REFERENCES

- Araya (R. A.), Bowles (J. F. W.), and Simpson (P. R.), 1977. *Neues Jahrb. Mineral. Mh.* 461.
 Batsonov (S. S.), 1964. *J. Struct. Chem.* 5, 862.
 Bither (T. A.), Bouchard (R. J.), Cloud (W. H.), Donohue (P. C.), and Siemons (W. J.), 1968. *Inorg. Chem.* 7, 2208.
 Burns (R. G.) and Vaughan (D. J.), 1970. *Am. Mineral.* 55, 1576.
 Goodenough (J. B.), 1972. *J. Solid State Chem.* 5, 144.
 Harbeke (G.), 1968. *Phys. Status Solidi.* 27, 9.
 Henry (N. F. M.), 1977. Quantitative Data File of the IMA-COM. London (McCrone).
 Koritnig (S.), 1962. In Landolt Börnstein, II Band, 8 Teil (Optische Konstanten). New York, Berlin, Heidelberg (Springer-Verlag).
 Newnham (R. E.), 1975. *Structure-Property Relations*. New York, Berlin, Heidelberg (Springer-Verlag).
 Pearson (W. D.), 1965. *Z. Kristallogr.* 121, 449.
 Strens (R. G. J.), 1979. *Bull. Minéral.* 102, 308.
 — and Freer (R.), 1978. *Mineral. Mag.* 42, 19.
 — and Wood (B. J.), 1979. *Mineral. Mag.* 43, 347.
 Tossell (J. A.), 1977. *J. Chem. Phys.* 66, 5712.
 Vaughan (D. J.) and Craig (J. R.), 1978. *Mineral Chemistry of Metal Sulfides*. Cambridge University Press (Cambridge).
 Wendlandt (W. Wm.) and Hecht (H. G.), 1966. *Reflectance Spectroscopy*. New York, London, Sydney (Wiley).
 Wilson (J. A.) and Yoffe (A. D.), 1969. *Adv. Phys.* 18, 183.
 Wood (B. J.), 1971. Electronic Spectra of some Solid Solutions. Ph.D. thesis, University of Newcastle upon Tyne.
 Wuensch (B. J.), 1974. In P. H. Ribbe (ed.), *Sulfide Mineralogy*. Washington (Mineralogical Society of America).

[Manuscript accepted for publication 20 August 1979]